Effect of Cold Compression and Heat Treatment on Microstructure and Mechanical Properties of Al-Zn-Mg-Cu Alloy

Xiaodong ZHAO [1], Wenjie WANG [1], Yueping FANG [2], Yajie LI [1]*, Fengming QIN [1]

[1] *School of Materials Science and Engineering, Taiyuan University of Science and Technology, Taiyuan, 030024, PR China*
[2] *China National Erzhong Group Deyang Wanhang Die Forging Co.LTD, Deyang, 618000, PR China*

http://doi.org/10.5755/j02.ms.36394

Received 22 February 2024; accepted 16 April 2024

The microstructural evolution of Al-Zn-Mg-Cu alloy under different stress and aging temperature was studied using cold compression and heat treatment. The relationship between the process parameter and the microstructure of the material was analyzed by OM, EBSD, and TEM. The results showed that the grain size decreased and the recrystallization fraction increased with the increase of compression. Textures of <111>||X (cubic), <110>//Y, Goss have higher intensity after solution treatment, but their intensity and proportion also decrease with the increase of compression. η' is the main precipitate in the alloy aged at 140 °C, while η is the main precipitate in the alloy aged at 160°C. Precipitation coarsening and grain refinement affect the microhardness of the alloy together.
Keywords: Al-Zn-Mg-Cu alloy, thermomechanical treatment, precipitation behavior, microstructure, microhardness.

1. INTRODUCTION

In recent years, 7xxx Al-Zn-Mg-Cu high-strength aluminum alloy has become a key structural material in aerospace, ocean shipping, automobile manufacturing, and other fields due to its high specific strength, excellent corrosion resistance, good formability, and fatigue resistance [1]. Its advantages lie in its high alloying and heat treatment strengthening properties, especially the improvement of mechanical properties of a large number of nano precipitates produced by aging treatment [2]. For conventionally 7075 alloys, most of the strength in the strongest state is provided by nanoscale precipitates [3 – 5]. During aging treatment, the supersaturated solid solution is easy to decompose into a GP region, which is characterized by nano-scale vacancy-rich atomic clusters [6]. GP I is usually first formed on the {100} Al habit plane, and is considered to be a spherical cluster rich in Mg [7]. Accordingly, GP || is formed on the {111} Al habit plane and is a Zn rich atomic layer [8, 9]. With the increase of aging temperature or time, the GP region gradually transforms into semi coherent η' phase. The precipitated phase (lattice constant a = 0.496 nm, c = 1.402 nm) is a hexagonal lattice located on the {111} Al habit plane. The η' precipitates are considered to be the main strengthening phase in the aging process. The η phase is a stable precipitate produced by over aging, which is incoherent with the matrix. One potential method to achieve greater strength is to combine aging and deformation.

High-strength Al-Zn-Mg-Cu aluminum alloy has a broad application prospect, but its formability at room temperature is limited [10]. Cold compression and heat treatment is an effective strengthening and toughening process, and this combination also can facilitate synergies [11 – 13]. Cold deformation can increase fine precipitates and dislocations, thereby improving the strength of the alloy, while hot deformation can reduce the size of recrystallized grains and improve the ductility of the alloy [14, 15]. Therefore, the required mechanical properties can be obtained in age-hardening aluminum alloys by refining grains and controlling precipitation behavior through appropriate deformation methods, the combination of solution, and aging heat treatment processes. The non-uniformity of deformation caused by various crystal textures will also affect the plastic deformation ability of the material. Therefore, it is necessary to weaken the texture by solution treatment and refine the microstructure by recrystallization [16]. However, under the effect of large deformation processes such as extrusion/rolling, the main basic texture intensity will even be increased. Ling et al. [17] found that in the annealed 7075 aluminum alloy, strong Cubic, Goss, and Brass textures were formed, of which Cubic texture was the main texture component. At the same time, the Cu and P texture intensity decreased during annealing. However, the change mechanism and law of the types and contents of recrystallization texture after quenching are not very clear.

Based on the above literature analysis, it is found that many studies of Al-Zn-Mg-Cu alloy deformation is on the thermal deformation behavior, however, the research on cold forming and heat treatment of 7 series aluminum alloy has not formed a mature theoretical system. It can be found that complete dynamic recrystallization of the alloy is difficult during 7 series aluminum alloy, only at higher temperature and lower strain rate can the proportion of dynamic recrystallization be increased to a certain extent, and dynamic recovery plays a dominant role in the process of thermal deformation. This is because the aluminum alloy layer fault energy is high, and dislocation slip and climb are easy to occur under high temperature conditions, so the

* Corresponding author. Tel.: +86-18536672860.
E-mail: *2019021@tyust.edu.cn.* (Y. Li)

dislocation density is low and dynamic recrystallization is difficult. Compared with dynamic recrystallization, static recrystallization of aluminum alloy is easier to occur and can effectively achieve microstructure refinement. The static recrystallization temperature of Al-Zn-Mg-Cu alloy is generally lower than its solid solution temperature, so the solid solution treatment can complete the recrystallization of the cold deformed alloy, and at the same time, the precipitation phase is redissolved to form a saturated solid solution, and finally, the aging strengthening treatment is carried out. At the same time, the homogenization-cold deformation-aging process can also be used to organically integrate deformation and aging together, and coordinate the relationship between cold deformation and aging treatment by adjusting the process parameters. Therefore, in this paper, the changes on grain size, types and quantities of precipitated phases, texture components and intensity before and after solution treatment were discussed in detail under different deformation and aging temperatures. The relationship between process parameters, microstructure, and mechanical properties was determined.

2. MATERIAL AND METHODS

The material used in this paper is high-strength Al-Zn-Mg-Cu alloy, which is provided by Longma Aluminum Group Co. Ltd. The casting method of ingot is semi continuous casting, and its main chemical composition is shown in Table 1. Fig. 1 shows the original structure of as cast material, which is mainly composed of α-Al matrix is composed of a low melting point eutectic phase on the grain boundary and in the grain, and its average grain size is 103.31 μm.

Table 1. The chemical compositions of the Al alloys (wt.%)

Si	Fe	Cu	Mg	Cr	Zn	Ti	Zr	Al
0.078	0.130	1.62	2.56	0.23	5.50	0.10	0.033	Bal.

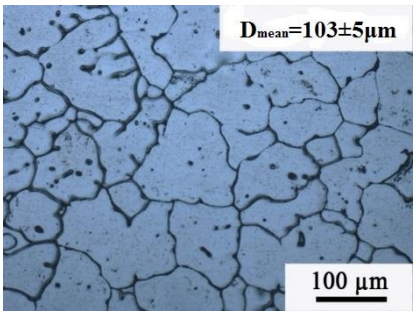

Fig. 1. The original microstructure of as-casted Al alloy

The eutectic phase at the grain boundary is basically distributed in a continuous network, and a large number of second phases are distributed at the grain boundary and in the crystal. The homogenization-cold deformation-solution-aging is used to process the material. The specific process route is shown in Fig. 2. First, the cubic ingot with dimensions of 100 mm × 100 mm × 100 mm was homogenized at 470 °C for 24 h, and then water cooled to room temperature. The cylindrical compression specimens with dimensions of φ 10 mm × 15 mm were compressed at room temperature on the universal testing machine, and the reduction is 10 %, 20 %, 30 %, and 40 %. Then, the compressed samples are subjected to solution and aging treatment. The solid solution treatment process was 470 °C, 0.5 h, followed by quenching by water cooling. The aging process is kept at 120 °C, 140 °C, and 160 °C for 24 hours, and then cooled at room temperature by air cooling. The heating speed of solution treatment and aging treatment is controlled at 20 °C/min.

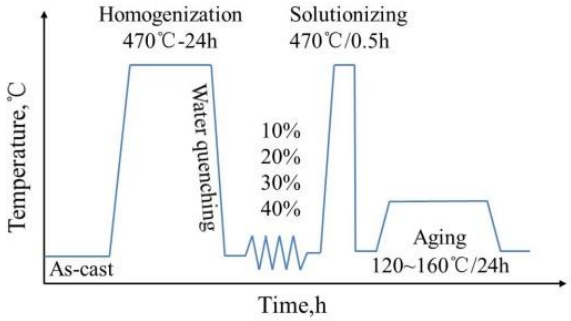

Fig. 2. Schematic diagram of the process in this study

The microstructure of the sample was analyzed by optical microscope (OM, Leica Microsystems Wetzlar GmbH, Germany), scanning electron microscope (SEM, Sirion 200), transmission electron microscope (TEM, FEI Tecnai G20), energy dispersive spectrometer (EDS) and electron backscatter diffraction analyzer (EBSD). OM and SEM observed that the samples were etched with Keller solution after mechanical polishing, and quantitative microstructure characterization was achieved using Image J software, including those measured by linear intercept method average grain size of α-Al. The grain size, grain shape, crystal orientation, and texture distribution of the samples were analyzed by EBSD and CHANNEL5 data processing software. After the EBSD observation sample is polished with 3000 mesh sandpaper, the 10 % perchloric acid ethanol solution is used for electrolytic polishing at -5 ℃. The step size of the EBSD data acquisition process is 1.0 μm. TEM and EDS were used to analyze the size and composition of precipitates. Grind the sample to about 40 μm. Then use 30 % nitric acid methanol solution to prepare TEM samples by electrolytic double spraying at -30 ℃. Fig. 3 shows a schematic diagram of sampling locations for microstructure observation. Finally, the XMD-100 microhardness tester was used to test the Vickers hardness of the sample, which is performed according to Metallic materials-Vickers hardness test standards (ISO 6507-1:2005) and takes the average value as the average hardness of the sample after five measurements.

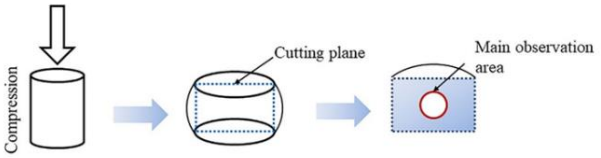

Fig. 3. The location of microstructure characterization

3. RESULTS AND DISCUSSION

3.1. Microstructure

Fig. 4 shows the microstructure of Al-Zn-Mg-Cu alloy

homogenized at 470 °C for 24 h. It can be seen from the microstructure shown in Fig. 4a that the number of non-equilibrium solidified eutectic phases after homogenization is significantly reduced, but a small part of eutectic phases still exist between the grains, which is speculated to be insoluble Fe rich phase and Si rich phase generated by Fe, Si and other impurities introduced in the casting process. It can be seen from the IPF diagram shown in Fig. 4 b that the grains are basically equiaxed and the grain size has not changed significantly after homogenization (average grain size is 104.52 μm). In addition, there is no obvious texture.

Fig. 5 shows the microstructure of Al-Zn-Mg-Cu alloy after compression with different deformation. It can be seen that the grains change from the original equiaxed grains to elongated flat grains under the effect of external stress. When the deformation is 10 %, there is no obvious change in the grain, as shown in Fig. 5 a. With the increase of deformation, many slip bands appear in the deformed grains, and the density and number of slip bands increase gradually, as shown in Fig. 5 b – d. The forming of numerous parallel slip lines is caused by the severe local plastic deformation that occurred in the grain interior. Moreover, it can be seen that these slip lines originate from GB regions with obvious wrinkles [18].

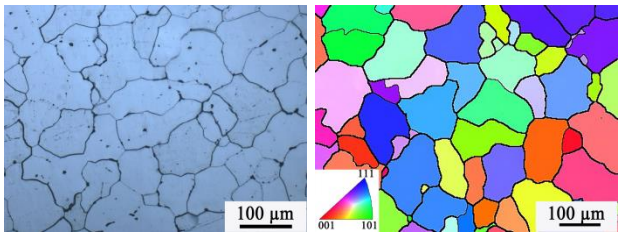

a b

Fig. 4. The microstructure of Al-Zn-Mg-Cu alloy after homogenization treatment: a – OM; b – IPF

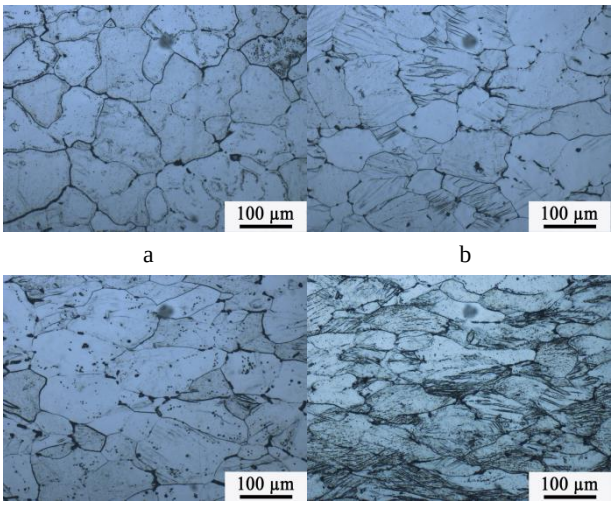

a b

c d

Fig. 5. Microstructure of Al-Zn-Mg-Cu after compression: a – 10 %; b – 20 %; c – 30 %; d – 40 %

Fig. 6 shows the microstructure of the deformed Al-Zn-Mg-Cu alloy specimen after solution treatment. After solution treatment, the microstructure undergoes different degrees of recrystallization. When the deformation is 10 % and 20 %, the recrystallized grains and the deformed grains show a mixed crystal state, as shown in Fig. 6 a, b. With the increase of deformation degree, the large deformed grains in the microstructure decrease, the fine recrystallized equiaxed new grains are more evenly distributed, and the effect of grain refinement is more obvious, as shown in Fig. 6 c, d. It decreases obviously with the increase of deformation degree. The recrystallization process includes the nucleation and growth of the new grains, which also requires the later heat treatment to provide a driving force to complete. The grain size change after heat treatment is related to the recrystallization nucleation rate and grain growth rate. The increase in deformation leads to the increase of material distortion energy, that is, the driving force for nucleation and growth increases, the recrystallization nucleation rate density increases, and the grains become finer.

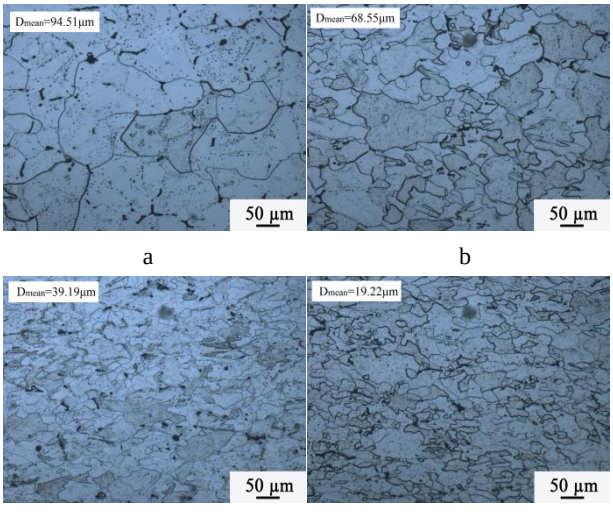

a b

c d

Fig. 6. Microstructure of Al-Zn-Mg-Cu alloy after solution treatment under different compression: a – 10 %; b – 20 %; c – 30 %; d – 40 %

Fig. 7 shows the TEM diagram of Al-Zn-Mg-Cu alloy after 30 % deformation and solution treatment. It can be seen from Fig. 7 a that deformation at room temperature causes a large number of dislocations in the grains to aggregate and form dislocation entanglement.

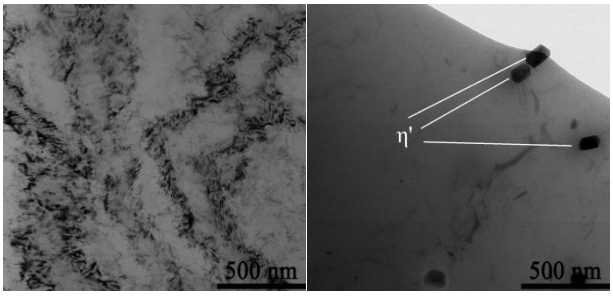

a b

Fig. 7. TEM diagram of Al-Zn-Mg-Cu alloy after different treatments: a – 30 % deformation; b – 30 % deformation and solution treatment

However, after solid solution treatment, the high density dislocation basically disappeared and some η' phases (verified by TEM in the following chapters) appeared (Fig. 7 b). Dislocations and subcrystals generated in the compression process serve as the recrystallization core and are consumed by the static recrystallization mechanism in the solution treatment process [19].

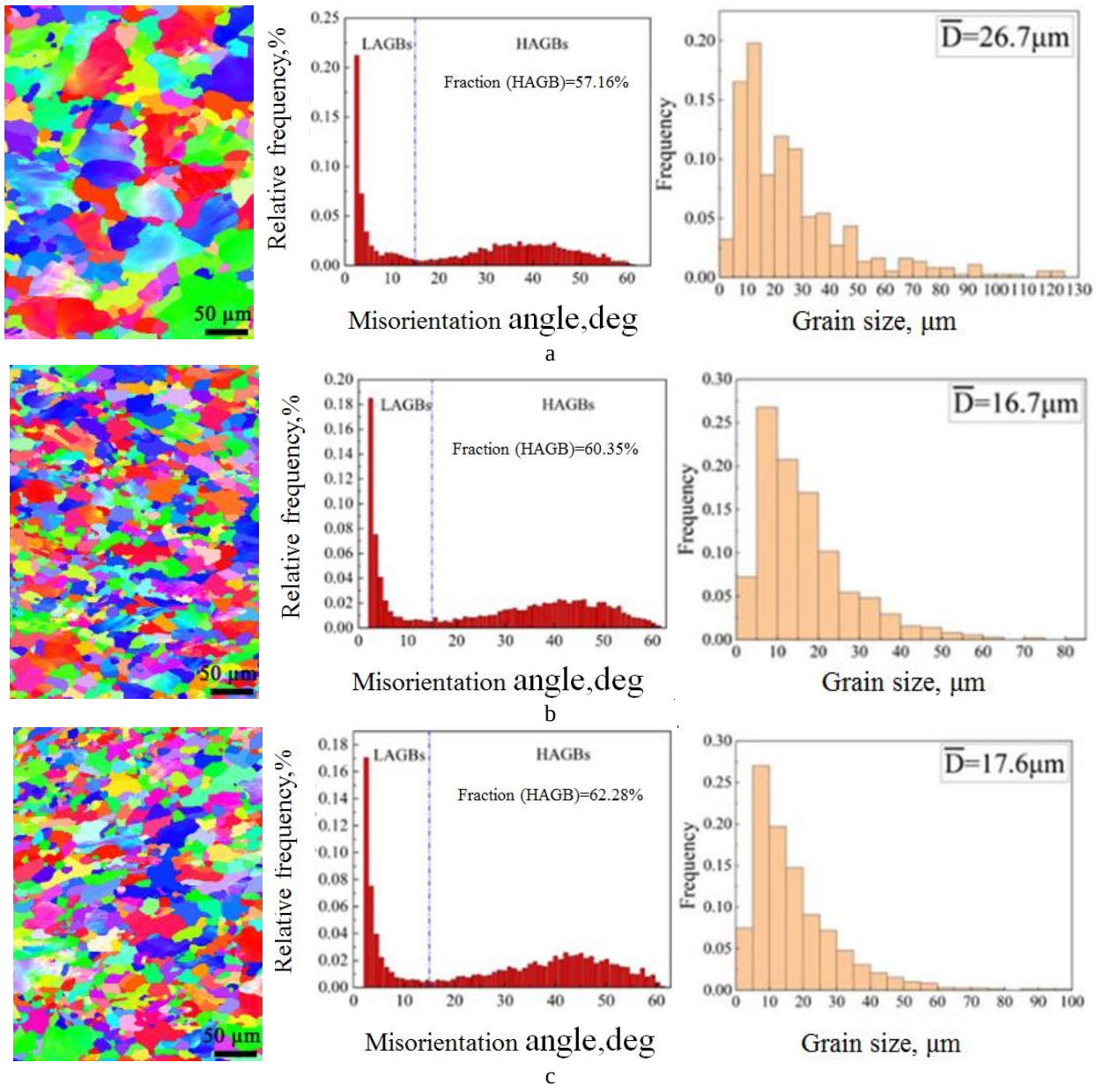

Fig. 8. IPF diagram and misorientation distribution diagram of Al-Zn-Mg-Cu alloy after solution treatment with different compression: a – 20 %; b – 30 %; c – 40 %

When the compression is 10 % and 20 %, the dislocation density introduced by a smaller deformation degree is lower, resulting in uneven recrystallization and a mixed crystal state. When the compression is 30 % and 40 %, the large deformation introduces high-density and relatively uniform dislocation [20], and the increase inf nucleation density makes the recrystallized grains more uniform and finer.

Fig. 8 shows the EBSD analysis diagrams of Al-Zn-Mg-Cu alloy deformed sample after solution treatment. It can be seen that the grain size and morphology of the three samples are quite different, and the grain presents a slender deformation state. Because the deformation amount is relatively small and the degree of recrystallization is low, the fully recrystallized structure with uniform refinement is not obtained, as shown in the IFP diagram. The results of EBSD show that the average grain size is 26.7 μm, 16.7 μm and 17.6 μm when the deformation amount is 20 %, 30 % and 40 %, respectively. The results show that 7075 aluminum alloy is subjected to large deformation (30 %) and solution treatment can significantly improve the recrystallization refining process. When the compressive deformation increases to 40 %, the degree of recrystallization does not increase significantly, but slightly decreases. At the same time, the grain boundary orientation distribution map shows the change rule of large and small angle boundaries. With the increase of compression deformation, the proportion of large angle grain boundaries increases, and the proportion of small angle grain boundaries correspondingly decreases. The proportion of high angle grain boundaries with deformation of 20 %, 30 %, and 40 % is 57.16 %, 60.35 % and 62.28 %, respectively. It indicates that the degree of recrystallization continues to increase, and the grain boundary orientation distribution map reflects the characteristics of continuous recrystallization [21].

Fig. 9 shows the orientation distribution function (ODF) diagram of samples with different compression amounts after solution treatment. The common deformation textures of cubic metal sheets are Cube{001}<100>, Goss{011}<100>, Copper{112}<111>, P{011}<112>, S{123}<634>and Brass{011}<211>. However, the texture types will be obviously different with different deformation modes. It can be seen from Fig. 9 that the texture types in the samples after compression deformation adopted in this paper are <111>||X(cubic), <110>//Y, and Goss respectively. Compared with alloys with dense Cube texture, alloys with dense Goss texture show excellent grain structure stability and smaller grain size [21]. The MRDs of <111>||X (cubic), <110>//Y, Goss are 3.41, 6.02, 5.50 when the compression is 20 %, 2.18, 3.78, 2.50 when the compression is 30 %, and 1.86, 3.12, 3.39 when the compression is 40 %. It can be seen that the overall change trend of MRD of <111>||X (cubic), <110>//Y, Goss decreases with the increase of compression, which is similar to the research results of Shaha et al [22].

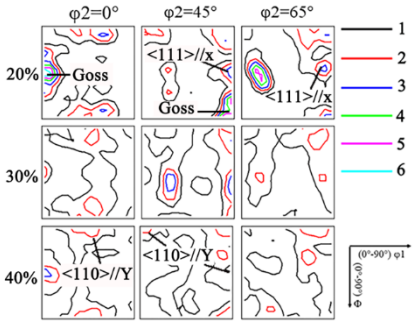

Fig. 9. ODF diagram of samples with different compression amounts after solution treatment (Y-compression direction, X-transverse direction)

Different textures can be easily calibrated in EBSD, and the change of grain orientation can be observed more intuitively through texture distribution. Fig. 10 shows the main texture distribution and recrystallization of samples with different compressions after solution treatment. Different colors are used to represent the typical texture in the sample, purple represents <110>//Y, green represents <111>||X(cubic), light blue represents Goss, and other areas that do not belong to the typical texture of the sample are defined as random textures and represented in white. When calculating the area fraction of each texture, an angle deviation of 15° is selected. For the recrystallization diagram, dark blue represents recrystallized grains, yellow represents recovered grains, and red represents deformed grains. The white line represents the small angle grain boundary (2°~15°), and the black line represents the large angle grain boundary (> 15°). Fig. 11 shows the statistical results of texture and recrystallization fraction. The results in Fig. 10 and Fig. 11 show that when the compression is 20 %, there are deformed grains and recovery grains with content of 45.7 % and 10.8 %, and recrystallization grains with content of 43.6 %. The recrystallized grains basically show a white random texture. <111>||X (cubic), <110>//Y, Goss oriented grains are mostly deformed grains and recovered grains, and a small amount of recrystallized grains. The area fraction of < 111>||X (cubic), <110>//Y and Goss are 19.5 %, 43.8 %, and 8.62 % respectively. With the increase of compression, when the deformation is 30 %, the proportions of deformed grains, recovered grains and recrystallized grains are 26 %, 2.75 % and 71.3 % respectively, indicating that the recrystallization degree increases. The area fraction of <111>||X (cubic), <110>//Y and Goss are 17.3 %, 36.3 %, and 3.54 %, which greatly reduce the content of texture compared with 20 %. When the deformation is 40%, the proportions of deformed grains, recovered grains and recrystallized grains are 31.9 %, 2.54 %, and 65.6 % respectively, and the area fraction of <111>||X (cubic), <110>//Y and Goss are 17.3 %, 27.9 %, and 5.05 % respectively. By comparing the grain proportion and texture fraction for 20 %, 30 %, and 40 % of deformation, it is not difficult to get such a view that after solution treatment, the recrystallization proportion always increases with the increase of compression, while the total texture content decreases. Meanwhile, when the deformation is 20 %, <111>||X (cubic), <110>//Y, Goss oriented grains are mostly deformed grains, but when the deformation is 30 % and 40 %, the content of typical textures in recrystallized grains is increased. The recrystallized grains (blue grain in Fig. 10 d, e and f) tend to increase with the increase of deformation, but the recrystallization grains (white grain in Fig. 10 a, b and c) with the random orientation are obviously higher than that in the samples with low deformation amount. In other words, the larger deformation weakens the texture of the aluminum alloy to a certain extent.

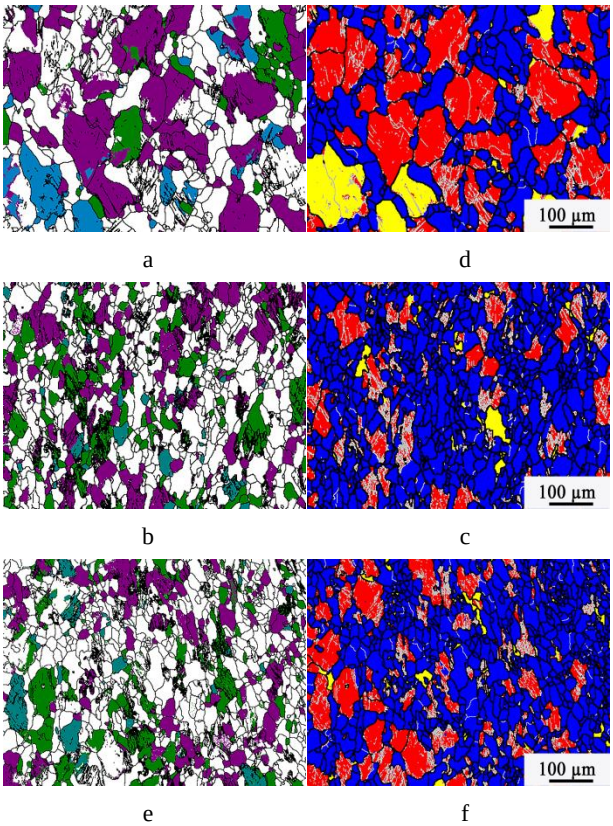

Fig. 10. Texture distribution and recrystallization diagram of samples with different compression amounts after solution treatment: a, b, c – 20 %, 30 %, 40 % texture distribution diagram; d, e, f – 20 %, 30 %, 40 % recrystallization diagram

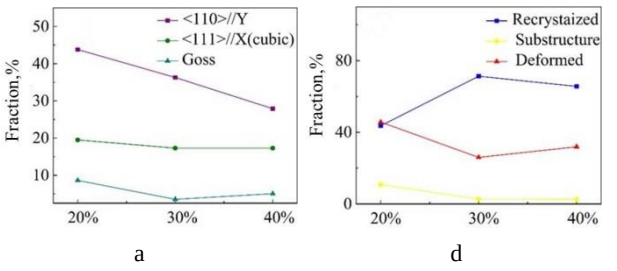

Fig. 11. Comparison analysis of samples with different compression amount after solution treatment: a – fraction of different textures; b – fraction of different grains

3.2. Precipitation behavior

By comparing the OM microstructure of aging treatment and solid solution treatment, we found no obvious change in grain size, so we mainly focused on studying the evolution law of nano-precipitated phase. Fig. 12 shows the precipitates and microstructure of Al-Zn-Mg-Cu alloy at the aging temperature of 140 °C. First, it can be observed that the discontinuous precipitates on the grain boundary are η phase precipitates. A large number of black η' metastable precipitates are distributed on both sides of the grain boundary, and their size is much smaller than that of the η precipitates [23, 24]. On both sides of the grain boundary, the width measured is about 80 ~ 90 nm, which is called the precipitation free zone (PFZ). The width of PFZ is related to the density of sediment or the total solute content. Alloys with high sediment density have smaller PFZ widths than those with low sediment density, which is a feature of solute depletion in PFZ [25, 26].

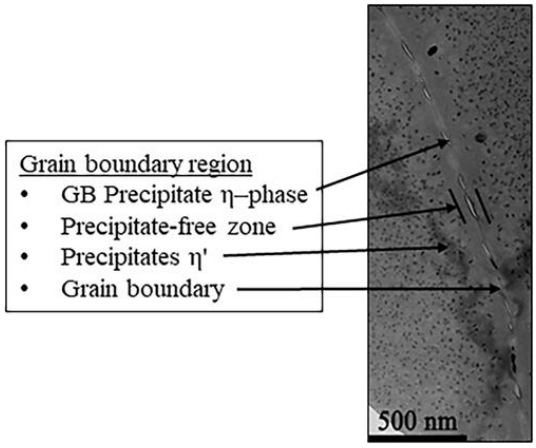

Fig. 12. TEM diagram of Al-Zn-Mg-Cu alloy at the aging temperature of 140°C

Fig. 13 shows the microscopic morphology of the sample at different aging temperatures. When the aging temperature is 140 °C, a large number of uniformly dispersed precipitates are precipitated in the matrix. At the same time, the average diameter of the precipitates is measured to be 9.6 nm. It is believed that after the aging is completed, the precipitates in the sample are mainly η' phase. When the aging temperature is 160 °C, a large number of precipitates are also precipitated in the matrix, and the morphology of these precipitates is basically spherical, but their size is far larger than the precipitates precipitated at 140 °C.

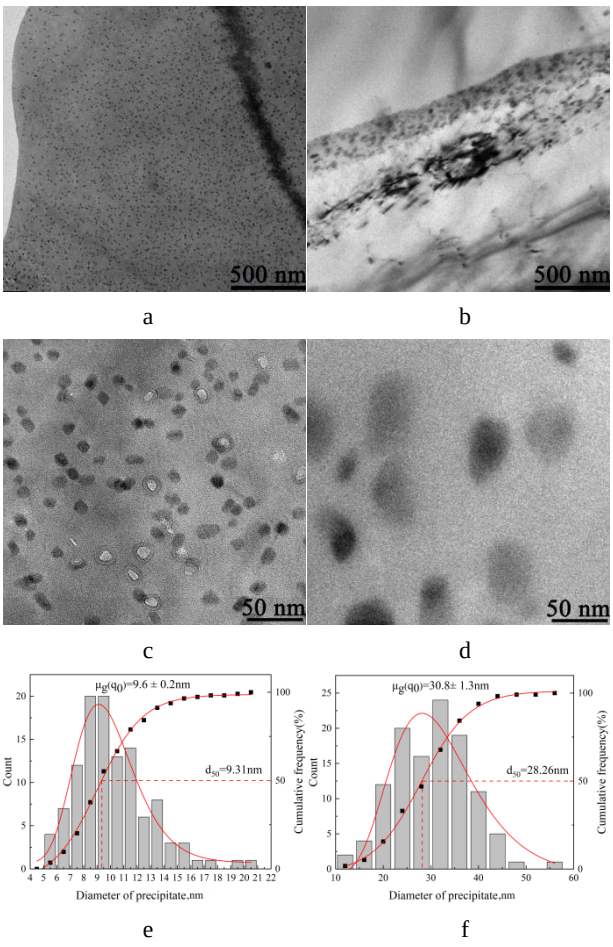

Fig. 13. The micro-morphology and particle size statistic diagram of Al-Zn-Mg-Cu alloy at different aging temperatures: a, c, e – 140 °C; b, d, f – 160 °C

The average diameter is 30.8 nm, and the size distribution is observed. It is believed that the precipitates are mainly the η phase. Significant coarsening of precipitates results in a significant reduction in the density of precipitates [6]. With the increase of aging temperature, the size of precipitates in the crystal gradually increases, and the type of precipitates also undergoes phase transformation.

Fig. 14 shows the TEM analysis results of the alloy after aging. Fig. 14 a shows the EDS results after aging at 140 °C. It can be seen that the precipitates are mainly Zn rich phase and Mg rich phase. Al element exists widely in the matrix, while Cu element does not appear obviously in the precipitation phase. According to the spectrogram in Fig. 14 b, it can be seen that the atomic ratio of Zn to Mg is 1.2. Similar to the results measured by 3D-APT [7], the atomic ratio of the η' phase is usually in the range of 1 to 1.3. It can be seen from the four crystallographic variants of the η' phase [27], that the precipitated phase is Mg2Zn3Al4.

Based on the results of microstructure and texture analyses, there are two typical recrystallization mechanisms, oriented nucleation and particle stimulated nucleation. The formation of large-angle boundaries based on texture evolution only occurs after a large deformation, and it is known that the large-angle boundaries gradually increase with rising strain [28], which is also consistent with the observations in Fig. 8. Therefore, more recrystallization

nucleation is induced by oriented nucleation during cold deformation and solution treatment, which refines the grains. The occurrence of PSN (particle-stimulated nucleation) within the grain or at the grain boundaries all contribute to the formation of the recrystallization texture [29]. However, Fig. 11 indicated that the typical texture fractions appear to decrease as the degree of recrystallization increases, indicating a higher proportion of recrystallized grains with random orientation rather than typical texture. It indicated that oriented nucleation plays a key role during cold deformation and heat treatment.

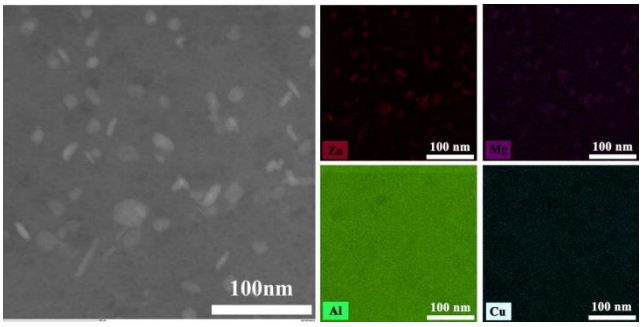

a

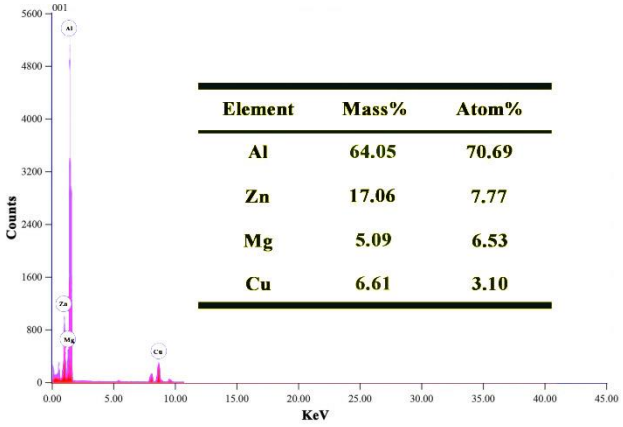

b

Fig. 14. TEM+ EDS of the alloy at the aging temperature of 140 °C: a – TEM morphology and EDS mapping; b – energy dispersion spectrum

3.3. Microhardness

Fig. 15 shows the changing trend of hardness under different process conditions. The variation trend of hardness is related to the grain size of the aluminum alloy under different deformation. In Fig. 15, after cold deformation and aging treatment, the hardness peaked with the increase of compression, and then gradually decreased. When the deformation was 30 % and the aging temperature was 140 °C, the peak value was 152 ± 2 HV, which is the maximum hardness value obtained under different deformation conditions. As the deformation amount increases from 20 % to 40 %, the grain size decreases obviously at first, and then increases slowly, and the average grain size is small (16.7 μm) at 30 % of the deformation amount (Fig. 8). Therefore, it can be seen from the hardness results that The increase of grain boundary improves the hardness of 7075 aluminum alloy to a certain extent. When the aging temperature increases to 160 °C with the deformation of 30 %, the hardness of the alloy decreases to 118 ± 10 HV. It can be seen from the precipitation behavior (Fig. 12 and Fig. 13) of the precipitated phase that the precipitated phase of the alloy is mainly η' under this process condition, which is considered to be the main reason for the 7xxx series aluminum alloy to obtain high strength and high hardness. The fine dispersed η' phase precipitates in large quantities and is evenly distributed in the structure, which increases the hardness of the alloy at the temperature of 140 °C. When the temperature increases to 160 °C, the main precipitated phase in the alloy is η, which can also produce a certain strengthening effect, but it is far inferior to η', so the hardness of the alloy decreases. The increase in aging temperature makes the hardness decrease, and the coarsening of precipitates is the main reason for this situation.

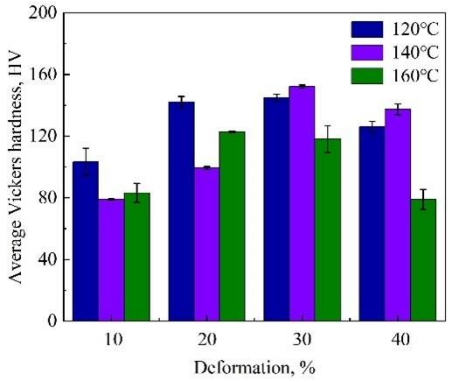

Fig. 15. Microhardness of Al-Zn-Mg-Cu alloy after aging

4. CONCLUSIONS

1. With the increase of compression, the grain size of Al-Zn-Mg-Cu alloy decreases gradually, and the number of slip bands in grains increases obviously. After solution treatment, the microstructure is obviously refined.
2. The overall intensity and proportion decrease with the increase of recrystallization degree, but <110>//Y always has a higher intensity. At the same time, the proportion of texture components in recrystallized grains increases with the increase of the recrystallization degree.
3. The aging temperature affects the average size of precipitates. At 140°C, the precipitates are mainly η' phase; At 160°C, the precipitated phase becomes η phase. The size difference between the precipitates lies in their nucleation and coarsening, and the temperature affects these two processes.
4. Both fine grain strengthening and precipitation strengthening will affect the hardness, but the hardness peak appears after solution treatment, indicating that the effect of fine grain strengthening on the hardness is not obvious. This phenomenon is caused by the dispersion distribution of the second phase in the precipitation process, and coarsening with the increase of temperature, resulting in a peak in hardness.

Acknowledgments

This work was financially supported by the Central government guides local funds for science and technology development (No.YDZJSX20231A045), Fundamental Research Program of Shanxi Province (No.202103021223288 and No.202103021224282).

REFERENCES

1. **Deng, Y.L., Zhang, Y.Y., Wan, L., Zhang, X.M.** Effects of Thermomechanical Processing on Production of Al-Zn-Mg-Cu Alloy Plate *Materials Science and Engineering A* 554 2012: pp. 33 – 40. https://doi.org/10.1016/j.msea.2012.05.102
2. **Lee, S.H., Jung, J.G., Baik, S.I., Park, S.H., Euh, K.** Effects of Ti Addition on The Microstructure and Mechanical Properties of Al-Zn-Mg-Cu-Zr Alloy *Materials Science and Engineering A* 801 2021: pp. 140437. https://doi.org/10.1016/j.msea.2020.140437
3. **Berg, L.K., Gjonnes, J., Hansen, V., Li, X.Z., Knutson-Wedel, M., Waterloo, G.** GP-zones in Al-Zn-Mg-Cu Alloys and Their Role in Artificial Aging *Acta Materialia* 49 (17) 2001: pp. 3443 – 3451. https://doi.org/10.1016/S1359-6454(01)00251-8
4. **Chung, T.F., Yang, Y.L., Shiojiri, M., Hsiao, C.N., Yang, J.R.** An Atomic Scale Structural Investigation of Nanometre-sized η Precipitates in The 7050 Aluminium Alloy *Acta Materialia* 174 2019: pp. 351 – 368. https://10.1016/j.actamat.2019.05.041
5. **Li, Q.L., Qin, J., Jiang, D.P., Yi, D.Q., Wang, B.** Precipitate Coarsening and Mechanical Properties in 6082 Aluminium Alloy During Long-term Thermal Exposure *Journal of Alloys and Compounds* 909 2022: pp. 164819. https://10.1016/j.jallcom.2022.164819
6. **Tang, J., Liu, M., Bo, G., Jiang, F., Luo, C., Teng, J., Fu, D., Zhang, H.** Unraveling Precipitation Evolution and Strengthening Function of The Al-Zn-Mg-Cu Alloys with Various Zn Contents: Multiple Experiments and Integrated Internal-state-variable Modelling *Journal of Materials Science & Technology* 116 2022: pp. 130 – 150. https://doi.org/10.1016/j.jmst.2021.12.008
7. **Sha, G., Cerezo, A.** Early-stage Precipitation in Al-Zn-Mg-Cu Alloy (7050) *Acta Materialia* 52 (15) 2004: 4503 – 4516. https://doi.org/10.1016/j.actamat.2004.06.025
8. **Wolverton, C.** Crystal Structure and Stability of Complex Precipitate Phases in Al-Cu-Mg-(Si) and Al-Zn-Mg Alloys *Acta Materialia* 49 (16) 2001: pp. 3129 – 3142. https://doi.org/10.1016/S1359-6454(01)00229-4
9. **Liu, Y., Jiang, D.M., Xie, W.L., Hu, J., Ma, B.R.** Solidification Phases and Their Evolution during Homogenization of a DC Cast Al-8.35Zn-2.5Mg-2.25Cu Alloy *Materials Characterization* 93 2014: pp. 173 – 183. https://doi.org/10.1016/j.matchar.2014.04.004
10. **Xu, L.Z., Zhan, L.H., Xu, Y.Q., Liu, C.H., Huang, M.H.** Thermomechanical Pretreatment of Al-Zn-Mg-Cu Alloy to Improve Formability and Performance during Creep-age Forming *Journal of Materials Processing Technology* 293 2021: pp. 117089. https://doi.org/10.1016/j.jmatprotec.2021.117089
11. **Huo, W.T., Hou, L.G., Cui, H., Zhuang, L.Z., Zhang, J.S.** Fine-grained AA 7075 Processed by Different Thermo-Mechanical Processings *Materials Science and Engineering A* 618 2014: pp. 244 – 253. https://doi.org/10.1016/j.msea.2014.09.026
12. **Huo, W.T., Shi, J.T., Hou, L.G., Zhang, J.S.** An Improved Thermo-mechanical Treatment of High-strength Al-Zn-Mg-Cu Alloy for Effective Grain Refinement and Ductility Modification *Journal of Materials Science & Technology* 239 2017: pp. 303 – 314. https://doi.org/10.1016/j.jmatprotec.2016.08.027
13. **Huang, Y.J., Chen, Z.G., Zheng, Z.Q.** A Conventional Thermo-mechanical Process of Al-Cu-Mg Alloy for Increasing Ductility While Maintaining High Strength *Scripta Materialia* 64 (5) 2011: pp. 382 – 385. https://doi.org/10.1016/j.scriptamat.2010.10.037
14. **Wang, D., Ma, Z.Y., Gao, Z.M.** Effects of Severe Cold Rolling on Tensile Properties and Stress Corrosion Cracking of 7050 Aluminum Alloy *Materials Chemistry and Physics* 117 (1) 2009: pp. 228 – 233. https://doi.org/10.1016/j.matchemphys.2009.05.048
15. **Huo, W.T., Hou, L.G., Lang, Y.G., Cui, H., Zhuang, L.Z., Zhang, J.S.** Improved Thermo-mechanical Processing for Effective Grain Refinement of High-strength AA 7050 Al alloy *Materials Science and Engineering A* 626 2015: pp. 86 – 93. https://doi.org/10.1016/j.msea.2014.12.071
16. **Hirsch, J., Al-Samman, T.** Superior Light Metals by Texture Engineering: Optimized Aluminum and Magnesium Alloys for Automotive Applications *Acta Materialia* 61 (3) 2013: pp. 818 – 843. https://doi.org/10.1016/j.actamat.2012.10.044
17. **Hua, L., Hu, X., Han, X.H.** Microstructure Evolution of Annealed 7075 Aluminum Alloy and Its Influence on Room-temperature Plasticity *Materials and Design* 196 2020: pp. 09192. https://doi.org/10.1016/j.matdes.2020.109192
18. **Chen, M.Y., Liu, S.D., He, K.H., Zheng, X., Jia, G.L.** The Effect of Precipitate-free Zone on Mechanical Properties in Al-Zn-Mg-Cu Aluminum Alloy: Strain-induced Back Stress Strengthening *Journal of Alloys and Compound* 969 2023: pp. 172426. https://doi.org/10.1016/j.jallcom.2023.172426
19. **Xiao, G.F., Jiang, J.F., Liu, Y.Z., Wang, Y., Guo, B.Y.** Recrystallization and Microstructure Evolution of Hot Extruded 7075 Aluminum Alloy during Semi-solid Isothermal Treatment *Materials Characterization* 156 2019: pp. 109874. https://doi.org/10.1016/j.matchar.2019.109874
20. **Wang, D., Huang, S.Q., Yi, Y.P., He, H.L., Li, C.** Effects of Cryogenic Deformation on The Microstructure and Mechanical Properties of High-strength Aluminum Alloys *Materials Characterization* 187 2022: pp. 111831. https://doi.org/10.1016/j.matchar.2022.111831
21. **Liu, F., Liu, Z.Y., He, G.Y., Ou, L.N.** Dislocation Ordering and Texture Strengthening of Naturally Aged Al-Cu-Mg Alloy *Journal of Materials Science & Technology* 118 2022: pp. 1 – 14. https://doi.org/10.1016/j.jmst.2021.12.011
22. **Shaha, S.K., Czerwinski, F., Kasprzak, W., Chen, D.L.** Work Hardening and Texture during Compression Deformation of The Al-Si-Cu-Mg Alloy Modified with V, Zr and Ti *Journal of Alloys and Compounds* 593 2014: pp. 290 – 299. https://doi.org/10.1016/j.jallcom.2013.12.081
23. **He, B.S., Cao, L.F., Wu, X.D., Tang, S.B., Lin, X.M., Zou, Y.** Effect of Continuous Retrogression and Re-ageing Treatment on Mechanical Properties, Corrosion Behavior and

Microstructure of an Al-Zn-Mg-Cu Alloy *Journal of Alloys and Compounds* 970 2024: pp. 17 – 28. https://doi.org/10.1016/j.jallcom.2023.172592

24. **Xiao, F., Shu, D., Wang, D.H., Zhu, G.L., Wang, S.B., Sun, B.D.** Effect of Zn Content on The Formability and Aging Precipitation of Al-Zn-Mg-Cu-Nb Alloys Prepared by LPBF *Journal of Materials Research and Technology* 25 |2023: pp. 6338 – 6335. https://doi.org/10.1016/j.jmrt.2023.07.057
25. **Zou, Y., Wu, X.D., Tang, S.B., Zhu, Q.Q., Song, H., Guo, M.X., Cao, L.F.** Investigation on Microstructure and Mechanical Properties of Al-Zn-Mg-Cu Alloys with Various Zn/Mg Ratios *Journal of Materials Science & Technology* 85 2021: pp. 106 – 117. https://doi.org/10.1016/j.jmst.2020.12.045
26. **Zhao, H., Geuser, F.D., Silva, A.K., Szczepaniak, A., Gault, B., Ponge, D., Raabe, D.** Segregation Assisted Grain Boundary Precipitation in a Model Al-Zn-Mg-Cu Alloy *Acta Materialia* 156 2018: pp. 318 – 329. https://doi.org/10.1016/j.actamat.2018.07.003
27. **Cao, F.H., Zheng, J.X., Jiang, Y., Chen, B., Wang, Y.R., Hu, T.** Experimental and DFT Characterization of η' Nano-Phase and Its Interfaces in Al-Zn-Mg-Cu Alloys *Acta Materialia* 164 2019: pp. 207 – 219. https://doi.org/10.1016/j.actamat.2018.10.045
28. **Hughes, D.A., Hansen, N.** High Angle Boundaries Formed by Grain Subdivision Mechanisms *Acta Materialia* 45 1997: pp. 3871 – 3886. https://doi.org/10.1016/S1359-6454(97)00027-X
29. **Rosen, G.I., Juul-Jensen, D., Hughes, D.A., Hansen, N.** Microstructure and Local Crystallography of Cold Rolled Aluminium *Acta Materialia* 43 1995: pp. 2563 – 2579. https://doi.org/10.1016/0956-7151(94)00473-U